# Characterization of Novel Quaternary Chitosan Derivative Nanoparticles Loaded with Protein

**Ajun Wan,[1] Yan Sun,[1] Huili Li[2]**

[1]*School of Chemistry and Chemical Technology, Shanghai Jiao Tong University, Shanghai 200240, China*
[2]*School of Pharmacy, Shanghai Jiao Tong University, Shanghai 200240, China*

Received 16 July 2007; accepted 19 March 2008
DOI 10.1002/app.28792
Published online 8 July 2009 in Wiley InterScience (www.interscience.wiley.com).

**ABSTRACT:** The objective of this work was to characterize a novel quaternary chitosan derivative [*O*-(2-hydroxyl) propyl-3-trimethyl ammonium chitosan chloride (*O*-HTCC)] nanoparticle system. *O*-HTCC nanoparticles were prepared with a simple and mild ionic gelation method upon the addition of a sodium tripolyphosphate solution to a low-molecular-weight *O*-HTCC solution. Highly cationic chitosan nanoparticles were prepared. Bovine serum albumin (BSA), a model protein drug, was incorporated into the nanoparticles. The physicochemical properties of the nanoparticles were determined with transmission electron microscopy (TEM), scanning electron microscopy (SEM), Fourier transform infrared analysis, differential scanning calorimetry, and X-ray diffraction (XRD) patterns. The results showed that increasing the BSA concentration from 1.5 to 2.5 mg/mL promoted the BSA encapsulation efficiency from 57.3% to 87.5% and the loading capacity from 70.2% to 99.5%. Compared with the chitosan nanoparticles, the *O*-HTCC nanoparticles had lower burst release. TEM revealed that the BSA-loaded *O*-HTCC nanoparticles were smaller than the *O*-HTCC nanoparticles when the BSA concentration was 1.5 mg/mL; SEM showed that the size of the BSA-loaded *O*-HTCC nanoparticles was mostly affected by the BSA concentration, and the increase in size occurred with the concentration increasing. Thermograms and XRD of the BSA-loaded nanoparticles suggested that polyelectrolyte–protein interactions increased with the BSA concentration increasing and greater chain realignment in the BSA-loaded nanoparticles. © 2009 Wiley Periodicals, Inc. J Appl Polym Sci 114: 2639–2647, 2009

**Key words:** drug delivery systems; morphology; nanotechnology

## INTRODUCTION

Chitosan is a naturally occurring biopolymer composed of β-1,4-linked 2-acetamino-2-deoxy-D-glucopyranose and 2-amino-2-deoxy-D-glucopyranose. It is generally obtained by the alkaline deacetylation of chitin, which is the main component of the exoskeleton of crustaceans and the second most abundant biopolymer in nature after cellulose. Chitosan has received a great deal of attention for decades in medical and pharmaceutical applications because of its nontoxic, nonantigenic, biocompatible, and biodegradable properties, which have allowed its use in various medical areas such as topical ocular applications,[1] implantation,[2] and injections.[3] Several studies have indicated that chitosan is also bioadhesive.[4,5] Chitosan has amino groups and hydroxyl groups on its backbone, which on the one hand make chitosan itself hydrophilic and on the other hand impart to chitosan a polycationic property. The cationic character of chitosan has been suggested to be the main cause of the unique properties and activity of chitosan.[6] The positive charge of chitosan probably interacts with the negative charge on the mucosal surface. Furthermore, chitosan may stay on the membrane surface and not go through the membrane because of its high molecular weight; this results in no severe damage.[7] Protonation of the amino group allows the polymer to be solubilized in aqueous acids and to interact with negatively charged materials.[8] It is this functional group that enables the formation of chitosan nanoparticles by crosslinking and desolvation with cationic salts.[9]

Chitosan is a weak base, and a certain amount of acid is required to transform the glucosamine units into the positively charged, water-soluble form.[10] Consequently, at a neutral pH, most chitosan molecules will lose their charge and precipitate from solution. Studies have shown that only protonated, soluble chitosan can trigger the opening of tight junctions and thereby facilitate the paracellular

*Correspondence to:* A. Wan (wanajun@sjtu.edu.cn) or H. Li (lihl@sjtu.edu.cn).

Contract grant sponsor: National Natural Science Foundation of China; contract grant numbers: 20376045 and 20676079.

Contract grant sponsor: Nanometer Technology Program of the Science and Technology Committee of Shanghai; contract grant number: 0452nm037.

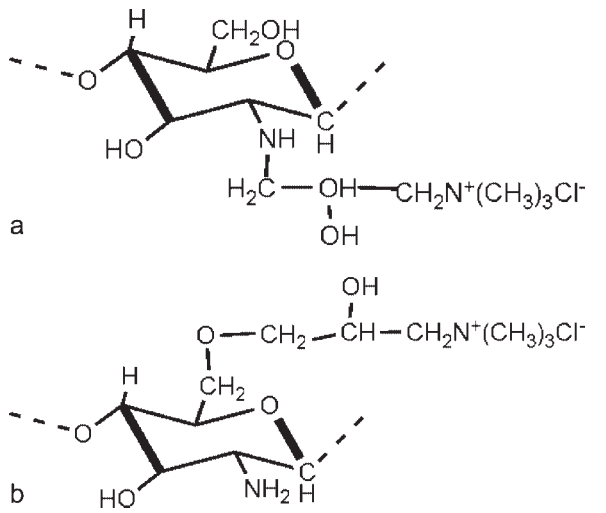


**Figure 1** Chemical structures of (A) HTCC and (B) *O*-HTCC.

transport of hydrophilic mannitol.[11] Chitosan derivatives with a quaternary ammonium moiety are thus interesting because a permanent cationic charge is gained on the polysaccharide backbone.[12] Also, the poor water solubility of chitosan can be enhanced by the attachment of a quaternary ammonium moiety to chitosan. Chitosan and chitosan salts lack the advantage of good solubility at neutral pH values. Chitosan aggregates in solutions at pH values above 6.5 and only protonated chitosan (i.e., in its uncoiled configuration) can trigger the opening of the tight junctions, thereby facilitating the paracellular transport of hydrophilic compounds.[13] This property implies that chitosan can be effective as an absorption enhancer only in a limited area of the intestinal lumen where the pH values are close to its pK. For this reason, chitosan and its salts may not be a suitable carrier for targeted peptide drug delivery to specific sites of the intestine, such as the jejunum or ileum. To overcome this problem, the chitosan derivative *N*-(2-hydroxyl) propyl-3-trimethyl ammonium chitosan chloride [HTCC; Fig. 1(A)] was synthesized,[14] and its nanoparticle system for paracellular transport was prepared. Quaternary chitosan derivatives have shown potential in various pharmaceutical applications, such as the delivery of peptides.[15–20] Compared with chitosan microspheres modified by reagents to introduce aliphatic and aromatic acyl groups, those quateraminated by glycidyl trimethylammonium chloride (GTMAC) displayed the highest adsorption of the antigen and indomethacin because of the strong electrostatic attraction of the quaternary aminonium group of HTCC to the negatively charged antigen and indomethacin.[21,22]

However, HTCC loses the positively charged amino group at the C-2 position of chitosan because of the chemical reaction of the amino group at the C-2 position and GTMAC [Fig. 1(A)]. To tackle this problem, a novel quaternary chitosan derivative, *O*-(2-hydroxyl) propyl-3-trimethyl ammonium chitosan chloride (*O*-HTCC), was prepared in our laboratory; it was synthesized by the coupling of GTMAC to chitosan, whose functional groups of the NH groups were protected. This compound was also perfectly soluble at neutral and basic pH values [Fig. 1(B)].

Therefore, the major goal of the work presented here was to create new more highly cationic nanoparticles and to evaluate their potential as protein carriers. Bovine serum albumin (BSA) is often chosen as a model protein for encapsulation studies in nanoparticles because of its well-known physicochemical properties and low cost.[23,24] BSA molecules that are amphoteric can form negatively charged nanospheres. Chitosan molecules contain amine and imine groups. The BSA concentration has an influence on improving the stability of BSA encapsulation efficiency and the loading capacity and on modulating its encapsulation and release property. The physicochemical structure of *O*-HTCC nanoparticles was analyzed with transmission electron microscopy (TEM), scanning electron microscopy (SEM), Fourier transform infrared (FTIR) analysis, differential scanning calorimetry (DSC), and X-ray diffraction (XRD) patterns. Our new method should find many applications in developing new chitosan-based biomedical materials carrying other drugs. In particular, our research may reveal the essence of the interaction between *O*-HTCC and protein drugs.

## EXPERIMENTAL

### Materials

Chitosan from shrimp shells was purchased from Jinhu Co., Ltd. (Jinhu City, Jiangsu Province, China); its deacetylation degree was 92%, and its weight-average molecular weight was 670 kDa. BSA with a weight-average molecular weight of 68 kDa was purchased from Sigma Chemical Co. (United States). GTMAC was obtained from Dongying Guofeng Fine Chemical Co., Ltd. (Shandong, China). All other chemicals were reagent-grade. *O*-HTCC was synthesized in our laboratory.[25]

### Preparation of chitosan nanoparticles, *O*-HTCC nanoparticles, and BSA-loaded nanoparticles

Chitosan and *O*-HTCC were dissolved in 1% acetic aqueous solutions adjusted to pH 5 at the same concentration of 2.5 mg/mL, respectively. Then, tripolyphosphate (TPP) was dissolved in distilled water at 2.5 mg/mL. Finally, 4 mL of the TPP solution was added to 20 mL of the chitosan solution or *O*-HTCC solution. An opalescent suspension was formed spontaneously under magnetic stirring at room

temperature, and it was further examined as nanoparticles.

BSA-loaded nanoparticles were formed upon the incorporation of TPP (2.5 mg/mL) into chitosan and *O*-HTCC solutions containing BSA (1.5, 2.0, and 2.5 mg/mL). An opalescent suspension was formed spontaneously under magnetic stirring at room temperature, and it was further examined as nanoparticles.

### Determination of the BSA encapsulation efficiency and loading capacity of the nanoparticles

The encapsulation efficiency and loading capacity of the nanoparticles of different forms were determined by ultracentrifugation of samples at 20,000*g* and 15°C for 30 min; the amount of free BSA was determined in the clear supernatant by UV spectrophotometry at 280 nm with the supernatant of nonloaded nanoparticles as a basic correction. The BSA loading capacity of the nanoparticles and the BSA encapsulation efficiency of the process were calculated with eqs. (1) and (2):

$$\text{BSA loading capacity} = (A - B)/C \times 100 \quad (1)$$

$$\text{BSA encapsulation efficiency} = (A - B)/A \times 100 \quad (2)$$

where $A$ is the total amount of BSA, $B$ is the free amount of BSA, and $C$ is the nanoparticle weight.

### BSA release from the nanoparticles *in vitro*

The *in vitro* BSA release profiles of the chitosan and *O*-HTCC nanoparticles were determined as follows. The BSA-loaded nanoparticles, separated from an 18-mL suspension, were put into test tubes with 6 mL of a 0.2 mol/L phosphate-buffered saline cushion liquid and incubated at 37°C under stirring. At appropriate intervals, samples were ultracentrifuged, and 3 mL of the supernatant was replaced with fresh medium. The amount of BSA released from the nanoparticles was evaluated by UV spectrophotometry (Lambda 20, PerkinElmer, United States). The calibration curve was made with nonloaded BSA nanoparticles as a correction.

### Nanoparticle characterization

#### Morphology of the nanoparticles

The nanoparticulate system morphology, including the shape and occurrence of aggregation phenomena, was studied with TEM and SEM, respectively. TEM experiments were carried out on a Hitachi model 600 electron microscope at a 75-kV accelerating voltage. A droplet of the nanoparticle dispersion was placed onto a copper grid covered with carbon (JEM-100CX, JEOL, Tokyo, Japan). Samples of nanoparticles were mounted on metal stubs, gold-coated *in vacuo*, and then examined on an S-2150 scanning electron microscope (Hitachi).

#### FTIR spectroscopy

Transmission IR spectra of chitosan, *O*-HTCC, *O*-HTCC nanoparticles, BSA-loaded *O*-HTCC nanoparticles, and BSA were measured with an FTIR spectrophotometer. The FTIR spectra of the samples were recorded with an IR spectrometer (model Paragon 1000, PerkinElmer) in the wavelength range of 500–4000 $cm^{-1}$. Signal averages were obtained for 32 scans at a resolution of 4 $cm^{-1}$.

#### DSC analysis

The DSC thermograms of pure chitosan, *O*-HTCC, their nanoparticles, and their BSA-loaded nanoparticles were recorded on a PerkinElmer Pyris I. A sample of 2–6 mg was accurately weighed into a solid aluminum pan with the cover sealed. The measurements were performed under nitrogen at a constant heating rate of 20°C/min under constant purging of nitrogen at 20 mL/min. All samples were run in duplicate.

#### Powder XRD study

Powder XRD patterns of chitosan, chitosan nanoparticles, BSA-loaded chitosan nanoparticles, *O*-HTCC, *O*-HTCC nanoparticles, and BSA-loaded *O*-HTCC nanoparticles were measured with a powder X-ray diffractometer (model D/MAX 220/PC, Rigaku, Japan).

## RESULTS AND DISCUSSION

### Size and morphology of the chitosan and *O*-HTCC nanoparticles and the BSA-loaded nanoparticles

The preparation of the chitosan nanoparticles, *O*-HTCC nanoparticles, and BSA-loaded nanoparticles was based on an ionic gelation interaction between the positively charged polymer and negatively charged TPP at room temperature. The chitosan nanoparticles, *O*-HTCC nanoparticles, and BSA-loaded nanoparticles, as shown by TEM observation (Fig. 2), exhibited quite regular and close-to-spherical shapes. The chitosan nanoparticles [Fig. 2(A)] were about 20 nm in size and compact and spherical in shape. Compared with those of the chitosan nanoparticles, the surfaces of the nanoparticles of *O*-HTCC were fluffy, and the size of the *O*-HTCC nanoparticles increased to about 250 nm [Fig. 2(B)]. The size of the chitosan nanoparticles, which was nearly 20 nm, was hardly affected by the BSA

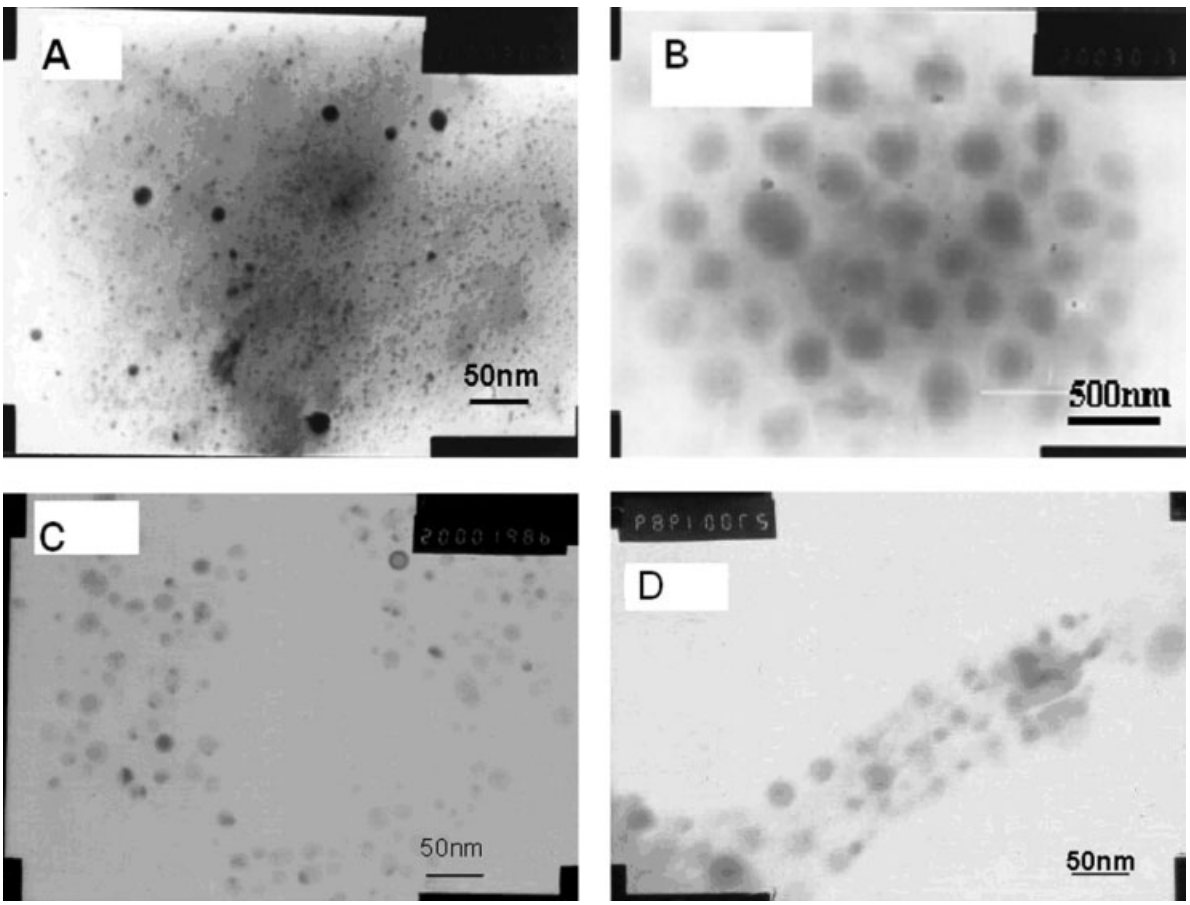


**Figure 2** TEM images of the nanoparticles: (A) chitosan, (B) *O*-HTCC, (C) BSA-loaded chitosan nanoparticles (1.5 mg/mL BSA), and (D) BSA-loaded *O*-HTCC nanoparticles (1.5 mg/mL BSA). A TPP concentration of 2.5 mg/mL was used.

loading, but the BSA-loaded nanoparticles of chitosan [Fig. 2(C)] exhibited an incompact and spherical shape in comparison with the chitosan nanoparticles. In contrast, the size and morphology of the *O*-HTCC nanoparticles were greatly affected by the BSA loading. After the loading of BSA, the size of the BSA-loaded *O*-HTCC nanoparticles [Fig. 2(D)] became smaller (ca. 30–50 nm) than that of the pure *O*-HTCC nanoparticles [ca. 250 nm; Fig. 2(B)] when the BSA concentration was 1.5 mg/mL. Because the isoelectric point of BSA is 4.8,[26] nanoparticles were prepared in an acid solution at pH 5.0. BSA is an anionic polymer whose $COO^-$ groups can interact strongly with $-N^+(CH_3)_3$ groups and $-CH-NH_3^+$ of *O*-HTCC. The similarity of the structures of BSA and chitosan led to a great interaction, which resulted in a strong interchain reaction and more compact formation. The BSA-loaded *O*-HTCC nanoparticles were slightly smaller than the pure *O*-HTCC nanoparticles, and this might have been due to the compact structure.

SEM observations of the pure *O*-HTCC nanoparticles [Fig. 3(A)] and BSA-loaded (1.5 mg/mL) *O*-HTCC nanoparticles [Fig. 3(B)] indicated that the size range of the BSA-loaded *O*-HTCC nanoparticles remained almost unchanged compared with that of the pure *O*-HTCC nanoparticles. The results were different from those of TEM because of BSA adsorption onto the nanoparticle surface during the freeze–dry process. SEM images [Fig. 3(A)] showed some small particles (ca. 100 nm) and a particle agglomerate. However, it is not clear if this was a result of the freeze–dry process or if it was a result of the sample preparation (the particle concentration of the sample) for SEM. With the BSA concentration increasing, the size of the BSA-loaded *O*-HTCC nanoparticles increased. The size of the BSA-loaded *O*-HTCC nanoparticles was nearly 125 nm when the BSA concentration was 1.5 mg/mL. We also observed BSA-loaded nanoparticles with sizes ranging from 250 nm [Fig. 3(C)] to about 1–3 μm [Fig. 3(D)] when the BSA concentration was changed from 2.0 to 2.5 mg/mL. There were two types of ionic interactions that contributed to the crosslinked networks of the BSA-loaded *O*-HTCC nanoparticles: the interaction between the junction formed by tripolyphosphoric groups and $-N^+(CH_3)_3$ and $-CH-NH_3^+$ groups of *O*-HTCC and the interaction between $COO^-$ of BSA and $-N^+(CH_3)_3$ and $-CH-NH_3^+$of *O*-HTCC.[26] Competition between

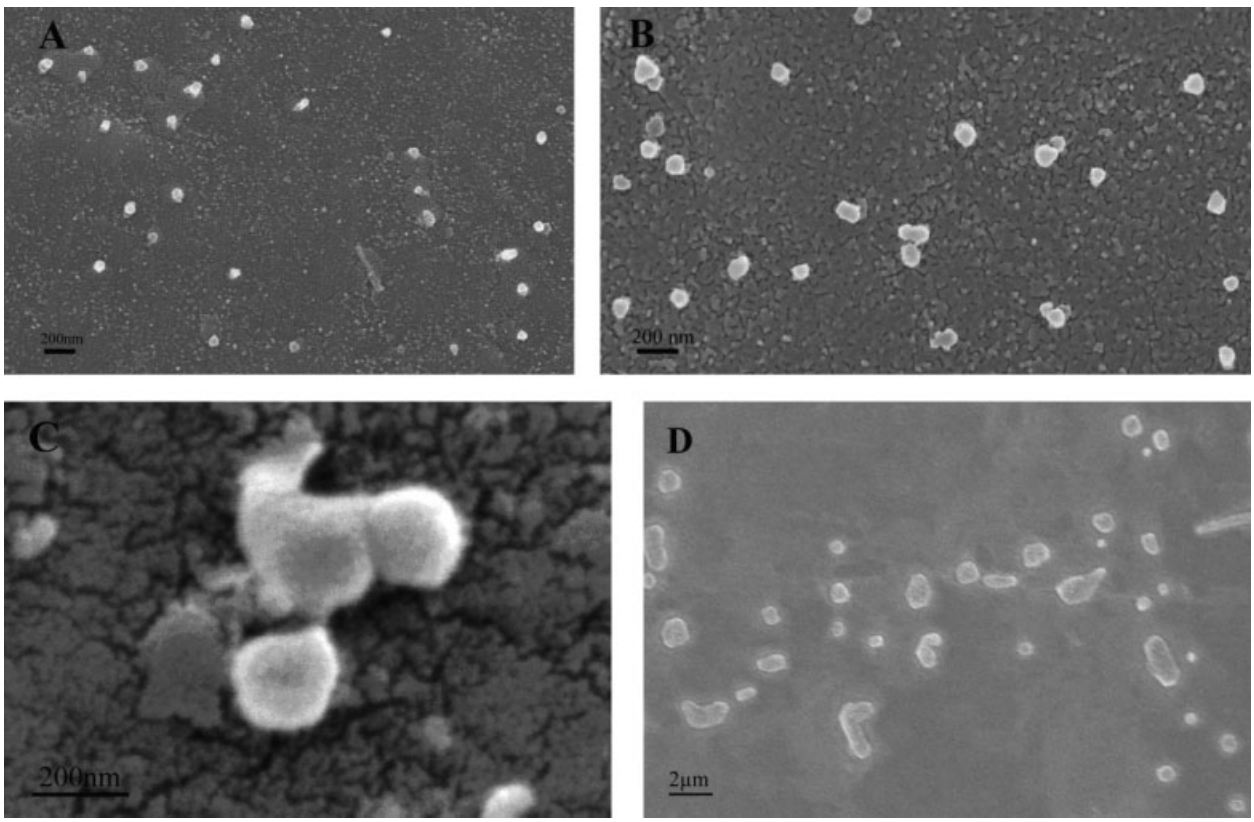


**Figure 3** SEM images of the nanoparticles: (A) pure *O*-HTCC, (B) BSA-loaded *O*-HTCC (1.5 mg/mL BSA), (C) BSA-loaded *O*-HTCC (2.0 mg/mL BSA), and (D) BSA-loaded *O*-HTCC (2.5 mg/mL BSA). A TPP concentration of 2.5 mg/mL was used.

TPP and BSA and physical encapsulation existed during the gelation process at the same time. Increasing the BSA concentration increased the interaction between BSA and *O*-HTCC and reduced the interaction between the junction formed by tripolyphosphoric groups and *O*-HTCC, so the size of the BSA-loaded *O*-HTCC nanoparticles increased, and the surfaces of the nanoparticles of *O*-HTCC appeared fluffy with the BSA concentration increasing.

### Encapsulation of BSA within the nanoparticles

As reported in Table I, the BSA encapsulation efficiency of the chitosan nanoparticles decreased from 45.7 to 20.4%: the lower the concentration, the higher the encapsulation efficiency. However, the BSA loading capacity was enhanced dramatically from 24.3 to 53% as the initial BSA concentration increased from 1.5 to 2.5 mg/mL. On the other hand, the BSA encapsulation efficiency and loading capacity of the *O*-HTCC nanoparticles were all increased. The BSA encapsulation efficiency was increased from 57.3% to 87.5%, and the loading capacity was increased from 70.2% to 99.5%, respectively, with the initial BSA concentration increasing from 1.5 to 2.5 mg/mL. That was because we prepared the nanoparticles in an acid solution at pH 5.0, which was above the isoelectric point of BSA (4.8), and *O*-HTCC had a more positive charge density than chitosan, which favored the interaction of BSA and *O*-HTCC.

### Release studies

The BSA *in vitro* release behavior of the chitosan and *O*-HTCC nanoparticles is shown in Figures 4 and 5. All release profiles of the nanoparticles were similar, exhibiting a small burst release in the first 10 h, but all the release profiles of the chitosan nanoparticles showed a larger burst (ca. 42.5%) than that of the *O*-HTCC nanoparticles (ca. 13.5–15.5%). Then, all the samples were followed by slow release at a constant but different rate. Moreover, the BSA concentration had a big effect on the release behavior of the

**TABLE I**
**Influence of the BSA Concentration on the Encapsulation Efficiency (AE) and Loading Capacity (LC)**

| BSA (mg/mL) | Chitosan | | *O*-HTCC | |
|---|---|---|---|---|
| | AE (%) | LC (%) | AE (%) | LC (%) |
| 1.5 | 45.7 | 24.3 | 57.3 | 70.2 |
| 2.5 | 20.4 | 53.0 | 87.5 | 99.5 |

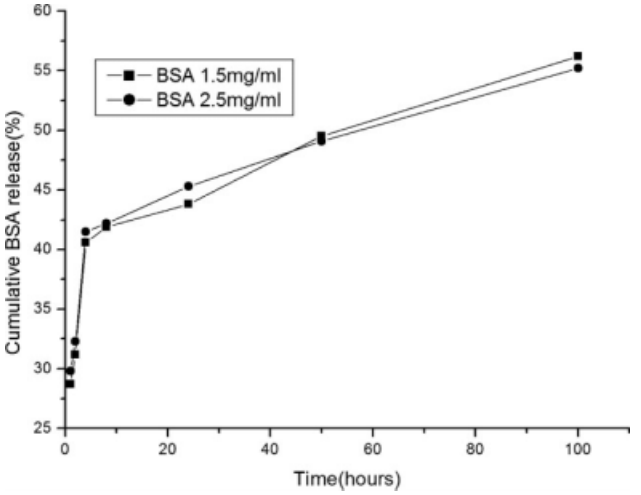


**Figure 4** Influence of the BSA concentration on the BSA release of chitosan.

BSA-loaded *O*-HTCC nanoparticles, in contrast to the results for the release behavior of the BSA-loaded chitosan nanoparticles. The BSA burst releases of chitosan and *O*-HTCC lasted several days because, on the one hand, the BSA molecular chain was much longer than the size of the nanoparticles, so it was difficult for BSA molecules to diffuse through the surface or pores of the nanoparticles in a short time, and on the other hand, the interaction between BSA and *O*-HTCC was stronger than that between BSA and chitosan, which also hindered BSA release from the nanoparticles.

## FTIR characterization

The FTIR spectra of chitosan, *O*-HTCC, *O*-HTCC nanoparticles, BSA-loaded *O*-HTCC nanoparticles, and BSA are shown in Figure 6. The absorption band at 1657 $cm^{-1}$ in native chitosan [Fig. 6(B)] was

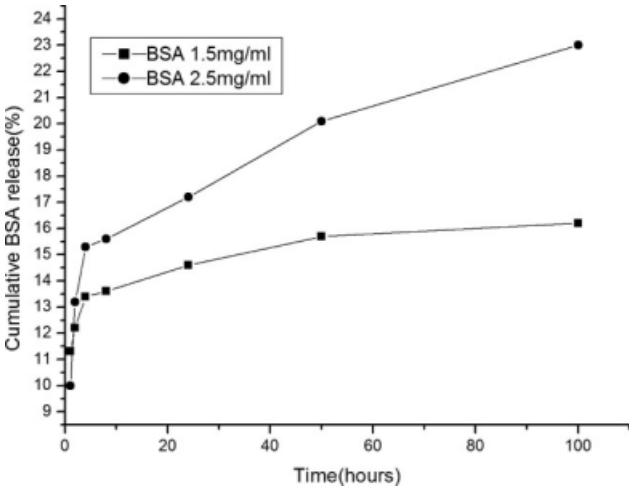


**Figure 5** Influence of the BSA concentration on the BSA release of *O*-HTCC.

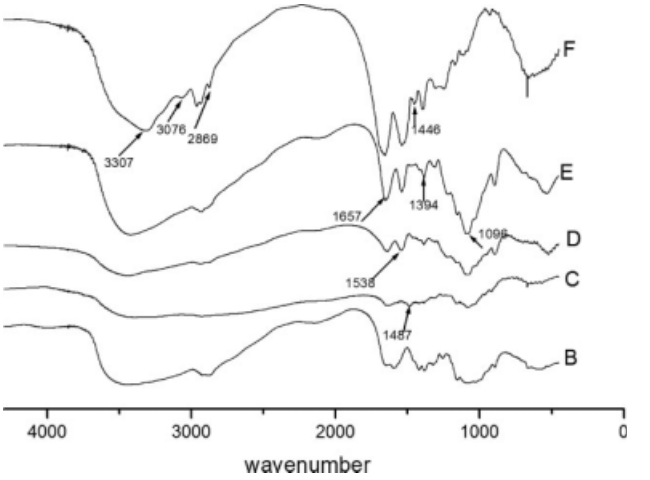


**Figure 6** IR spectra of the samples: (B) chitosan, (C) *O*-HTCC, (D) *O*-HTCC nanoparticles, (E) BSA-loaded *O*-HTCC nanoparticles, and (F) BSA.

referenced to amide I bands, whereas the absorption band at 1606 $cm^{-1}$ was ascribed to the N—H bending mode in the primary amine. The absorption band of $—NH_2$ in *O*-HTCC [Fig. 6(C)] still existed, and this suggested that N-alkylation in chitosan did not occur. Compared with chitosan, *O*-HTCC produced a new band at 1487 $cm^{-1}$, which was attributed to the methyl groups of ammonium.[27] In addition, the absorption band at 1096 $cm^{-1}$, which was caused by $CH_2—O—CH_2$ of *O*-HTCC, was very obvious. This indicated that the reaction happened. The spectrum of the *O*-HTCC nanoparticles [Fig. 6(D)] was different from that of the *O*-HTCC matrix. The intensity of the 1487-$cm^{-1}$ peak became weaker, and a new peak at 1538 $cm^{-1}$ appeared. The characteristic peaks of BSA had acetylamino I at 1657 $cm^{-1}$ and acetylamino II at 1538 and 3307 $cm^{-1}$ for $n(NH_2)$.[28] Acetylamino I at 1657 $cm^{-1}$ and acetylamino II at 1539 $cm^{-1}$ in BSA [Fig. 6(F)] overlapped 1657 $cm^{-1}$ of d(NH) and 1538 $cm^{-1}$ in nonloaded *O*-HTCC nanoparticles, so the more intensive peaks of both appeared for the BSA-loaded *O*-HTCC nanoparticles [Fig. 6(E)]. In addition, the characteristic peak of 1487 $cm^{-1}$ for *O*-HTCC became weak, and this was consistent with the result for the BSA-loaded HTCC nanoparticles.[26] We suppose that the tripolyphosphoric groups of TPP were linked with ammonium groups; at the same time, the intermolecular action and intramolecular action were enhanced in the *O*-HTCC nanoparticles.

## Thermal analysis

A PerkinElmer Pyris I differential scanning calorimeter was used. Each sample (2–6 mg) was run at a scanning rate of 20°C/min under a nitrogen atmosphere. The temperature for the first scan increased

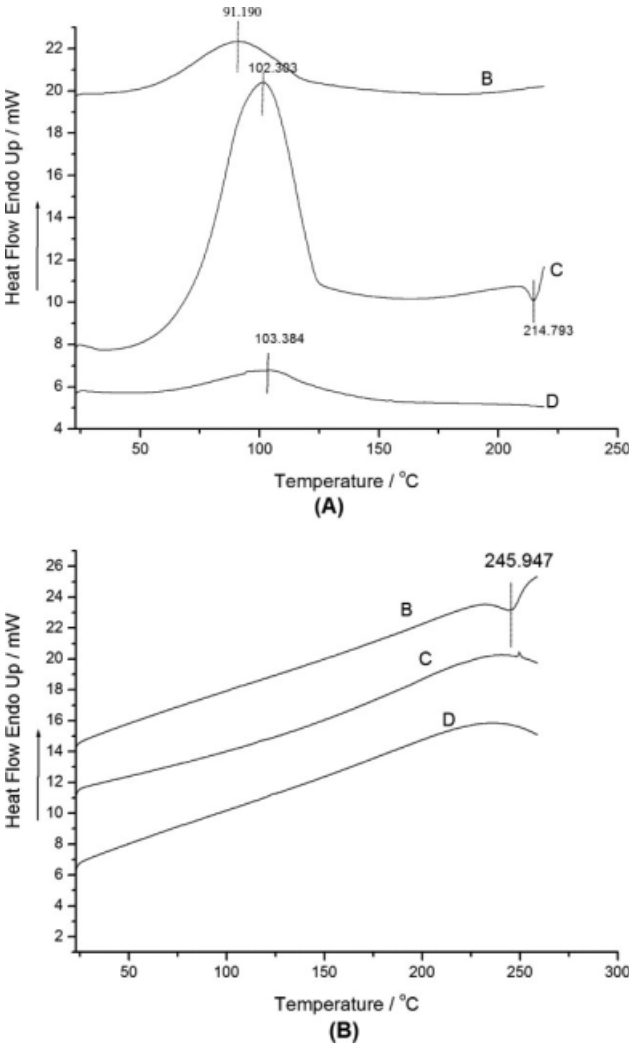


**Figure 7** DSC thermograms of (A) the first scan [(B) *O*-HTCC nanoparticles, (C) *O*-HTCC, and (D) chitosan] and (B) the second scan [(B) *O*-HTCC nanoparticles, (C) *O*-HTCC, and (D) chitosan].

from 20 to 220°C, then was held for 5 min at 220°C, and then was reduced from 220 to 20°C at 20°C/min; this was followed by immediate rescanning in the temperature range of 20–260°C. Polysaccharides usually have a strong affinity for water, and in the solid state, these macromolecules might have disordered structures that could be easily hydrated. Generally, the hydration properties of these polysaccharides depended on the primary and supramolecular structures, and the presence of bound water also had a strong influence on the overall polymorphic nature of the macromolecule. Therefore, the endotherm related to the evaporation of bound water was expected to reflect chemical and molecular changes during modifications.

Figure 7(A) reveals that there were differences in the endotherm peak area and position, indicating that these macromolecules differed in their water-holding capacity and the strength of the water–polymer interaction. The thermal peaks registered in all the samples were wide endotherm peaks centered between 55 and 125°C. The endotherm peak area and enthalpy ($\Delta H$) values of *O*-HTCC [Fig. 7(A)-C] were higher than those of chitosan [Fig. 7(A)-D]. Compared to *O*-HTCC, *O*-HTCC nanoparticles [Fig. 7(A)-B] had lower $\Delta H$ values, which indicated that the nanoparticles hindered water absorption. For the *O*-HTCC reference specimen, a small peak was observed at about 214.7°C. This revealed that *O*-HTCC decomposed slightly when the temperature reached 210°C. After the first scan, the free water was eliminated, and the different thermal transitions of each sample could be seen clearly in the spectra of the second scan [Fig. 7(B)]. In the DSC curve of the *O*-HTCC nanoparticles [second heating run; Fig. 7(B)-B], a new exothermic peak centered near 246°C was possibly linked to the decomposition procedure of the *O*-HTCC nanoparticles. Compared to *O*-HTCC [Fig. 7(A)-C], the *O*-HTCC nanoparticles [Fig. 7(B)-B] had a higher exothermic peak value, which indicated that ionic crosslinking hindered the decomposition of *O*-HTCC. No integrated exothermic peaks were observed in chitosan and *O*-HTCC in the second heating run, but at about 260°C, there was tendency that indicated the onset of chitosan degradation.[29]

Figure 8 shows the thermal transitions of BSA-loaded *O*-HTCC nanoparticles and BSA-loaded chitosan nanoparticles. For each case of BSA-loaded *O*-HTCC nanoparticles, a new well-defined exothermic peak appeared, which was consistent with simple cleavage of the substituent groups, which in some way might also involve backbone cleavage. The

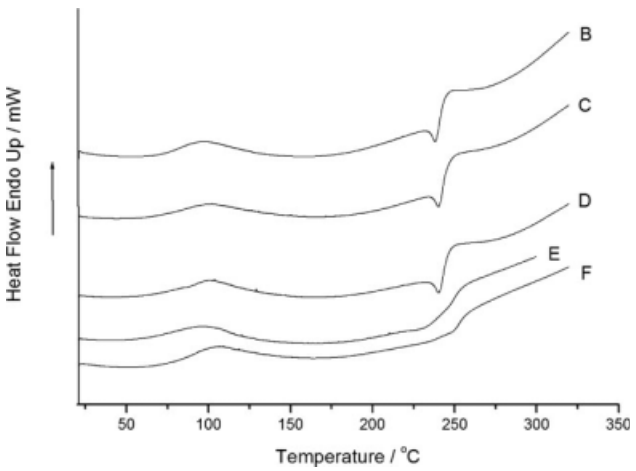


**Figure 8** DSC thermograms of BSA-loaded *O*-HTCC and chitosan nanoparticles: (B) *O*-HTCC (1.5 mg/mL BSA), (C) *O*-HTCC (2.0 mg/mL BSA), (D) *O*-HTCC (2.5 mg/mL BSA), (E) chitosan (1.5 mg/mL BSA), and (F) chitosan (2.5 mg/mL BSA).

analysis of the DSC curves for the BSA-loaded *O*-HTCC nanoparticles showed two additional endothermic peaks at about 230 and 250°C [Fig. 8(B–D)], in addition to the wide endothermic peak centralized between 95 and 103°C with an onset at 60°C. The peak at about 230°C was probably related to the breakdown of weak electrostatic interactions between BSA and *O*-HTCC.[30,31] With the BSA concentration increasing, the exothermic peak at about 235°C moved to a higher temperature; in contrast, the second endothermic peak moved to a lower temperature. These observations strongly supported the fact that increasing the BSA concentration increased the interaction between BSA and *O*-HTCC and reduced the interaction between the junction formed by tripolyphosphoric groups and *O*-HTCC. After the exothermic peak, for the BSA-loaded *O*-HTCC nanoparticles, there appeared a gradual change in the slope of the curve in the neighborhood of 242.16°C. The origin of this transition was attributed to the glass-transition temperature ($T_g$). The BSA concentration had little effect on the thermal transitions of the BSA-loaded *O*-HTCC nanoparticles. No evident exothermic peaks were observed in the BSA-loaded chitosan nanoparticles versus the BSA-loaded *O*-HTCC nanoparticles. However, in the case of the BSA-loaded chitosan nanoparticles discussed here, a clear $T_g$ was exhibited. Concerning $T_g$ of chitin and chitosan, it was predicted previously to be latent at a decomposition temperature greater than 230°C, as in the case of cellulose.[32] However, in the thermograms of the BSA-loaded chitosan nanoparticles (curves) shown in Figure 8(E,F), there are gradual changes in the slopes of the curves around 250°C. With the BSA concentration increasing, the $T_g$ value of the BSA-loaded chitosan nanoparticles increased to a rather higher temperature, and this suggested that the $T_g$ value of the BSA-loaded chitosan nanoparticles was highly affected by BSA. $T_g$ of the BSA-loaded chitosan nanoparticles was 235°C [Fig. 8(E)] when the BSA concentration was 1.5 mg/mL, and then $T_g$ of the BSA-loaded chitosan nanoparticles (2.5 mg/mL BSA) was 255°C [Fig. 8(F)]; this was higher by about 20°C than that of the BSA-loaded chitosan nanoparticles with the lower BSA concentration (1.5 mg/mL). The reason for this phenomenon might be that BSA and chitosan could form a weak ionic interaction between themselves, and then these interaction points could act as physical crosslinking points to increase the chain entanglement; thus, the chain movement of polyacrylamide was limited, and $T_g$ of polyacrylamide was increased.

## XRD analysis

Powder XRD patterns of chitosan, chitosan nanoparticles, *O*-HTCC, and *O*-HTCC nanoparticles are shown in Figure 9(A). There were two strong peaks in the diffractogram of chitosan at 2θ values of 10.4 and 21.8°, indicating the high degree of crystallinity of chitosan, their crystal lattice constants corresponding to 8.470 and 4.075, respectively.[33] However, no peak was found in the diffractograms of the chitosan nanoparticles, *O*-HTCC nanoparticles, and *O*-HTCC. Quaternary chitosan derivatives destroyed the degree of crystallinity of chitosan. There were no differences between the diffractograms of the chitosan nanoparticles and *O*-HTCC nanoparticles. XRD of the chitosan nanoparticles and *O*-HTCC nanoparticles was characteristic of an amorphous polymer. The nanoparticles were composed of a dense network structure of interpenetrating polymer chains crosslinked to one another by TPP counterions.[34] XRD implicated greater disarray in the chain alignment in the nanoparticles after the crosslinks.[33]

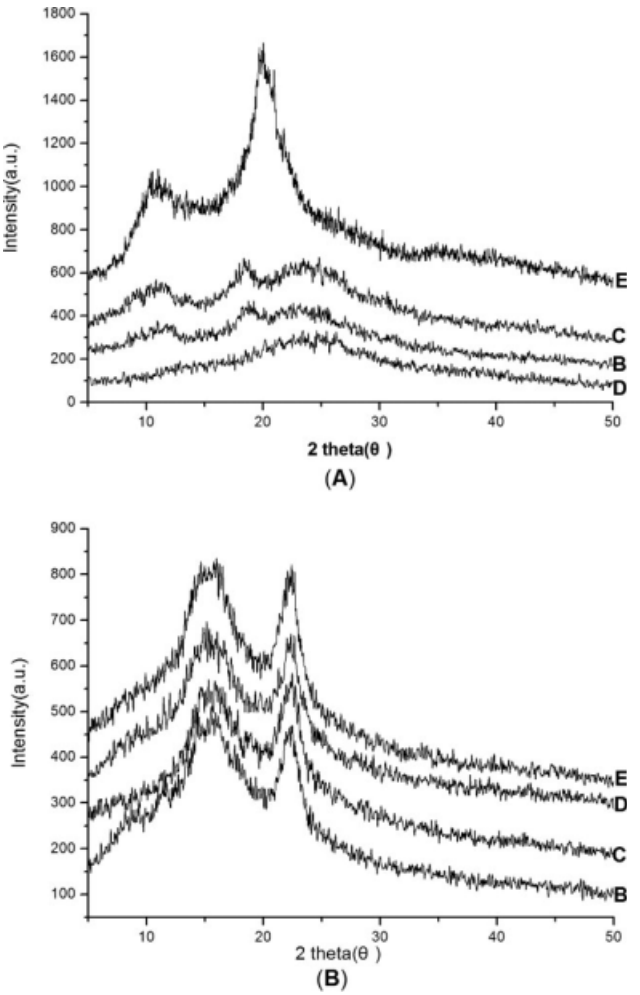


**Figure 9** XRD of (A)-B chitosan nanoparticles, (A)-C *O*-HTCC nanoparticles, (A)-D *O*-HTCC, (A)-E chitosan, (B)-B BSA-loaded chitosan nanoparticles (1.5 mg/mL BSA), (B)-C BSA-loaded *O*-HTCC nanoparticles (0.5 mg/mL BSA), (B)-D BSA-loaded *O*-HTCC nanoparticles (1.5 mg/mL BSA), and (B)-E BSA-loaded *O*-HTCC nanoparticles (2.5 mg/mL BSA).

Conversely, XRD implicated greater array in the chain alignment in the nanoparticles after the BSA loading and freeze drying [Fig. 9(B)]. There were two strong peaks in the diffractogram of the BSA-loaded nanoparticles at 2θ values of 15.5 and 22.5°, which showed that chain realignment happened during the BSA-loaded nanoparticle formation and growth, and this suggested a structure with an orderly molecular arrangement, the discovery of which has implications for BSA encapsulation and release mechanisms.[35]

## CONCLUSIONS

In this study, the physicochemical structure of *O*-HTCC nanoparticles was different from that of chitosan nanoparticles, and intermolecular and intramolecular actions were enhanced because of the gelation of tripolyphosphoric groups of TPP with cationic groups of chitosan and *O*-HTCC. After the loading of a low BSA concentration (1.5 mg/mL), the size of the *O*-HTCC nanoparticles became smaller; however, the higher the initial concentration was of BSA, the larger the size was of the BSA-loaded *O*-HTCC nanoparticles. The BSA concentration had a big effect on the release behavior of the BSA-loaded *O*-HTCC nanoparticles, and the protein encapsulation efficiency and loading capacity all increased with the initial BSA concentration increasing. FTIR, DSC, and XRD were successfully used to characterize the nanoparticulate and BSA-loaded nanoparticulate systems of chitosan and *O*-HTCC. XRD implicated greater array in the chain alignment in the nanoparticles after BSA loading and freeze drying.

## References


1. Felt, O.; Furrer, P.; Mayer, J. M.; Plazonnet, B.; Buri, P.; Gurny, R. Int J Pharm 1999, 180, 185.
2. Chatelet, C.; Damour, O.; Domard, A. Biomaterials 2001, 22, 261.
3. Grant, J.; Cho, J.; Allen, C. Langmuir 2006, 22, 4327.
4. He, P.; Davis, S. S. Int J Pharm 1998, 166, 75.
5. Calvo, P.; Vila-Jato, J. L.; Alonso, M. J. Int J Pharm 1997, 153, 41.
6. Anal, A. K.; Stevens, W. F. Int J Pharm 2005, 290, 45.
7. Natsume, H.; Iwata, S.; Ohtake, J.; Miyamoto, M.; Yamaguchi, M.; Hosoya, K. I.; Kobayashi, D.; Sugibayashi, K.; Morimoto, Y. Int J Pharm 1999, 185, 1.
8. Suheyla, K. H. J Microencapsul 1997, 14, 689.
9. Janes, K. A.; Calvo, P.; Alonso, M. J. Adv Drug Delivery Rev 2001, 47, 83.
10. Chandy, T.; Sharma, C. P. Artif Cells Artif Organs 1990, 18, 1.
11. Sinha, V. R.; Singla, A. K.; Wadhawan, S.; Kaushik, R.; Kumria, R.; Bansal, K.; Dhawan, S. Int J Pharm 2004, 74, 1.
12. Holappa, J.; Nevalainen, T.; Soininen, P.; Másson, M.; Järvinen, T. Biomacromolecules 2006, 7, 407.
13. Van der Lubben, I. M.; Verhoef, J. C.; Borchard, G.; Junginger, H. E. Eur J Pharm Sci 2001, 14, 201.
14. Wu, J.; Su, Z. G.; Ma, G. H. Int J Pharm 2006, 315, 1.
15. Thanou, M. M.; Verhoef, J. C.; Marbach, P.; Junginger, H. E. J Pharm Sci 2000, 89, 951.
16. Thanou, M. M.; Nihot, M. T.; Jansen, M.; Verhoef, J. C.; Junginger, H. E. J Pharm Sci 2001, 90, 38.
17. Thanou, M. M.; Verhoef, J. C.; Junginger, H. E. Adv Drug Delivery Rev 2001, 52, 117.
18. Kotzé, A. F.; de Leeuw, B. J.; Lueben, H. L.; de Boer, A. G.; Verhoef, J. C.; Junginger, H. E. Int J Pharm 1997, 159, 243.
19. Kotzé, A. F.; Thanou, M. M.; Lueben, H. L.; De-Boer, A. G.; Verhoef, J. C.; Junginger, H. E. J Pharm Sci 1999, 88, 253.
20. Nam, C. W.; Kim, Y. H.; Ko, S. W. J Appl Polym Sci 1999, 74, 2253.
21. Mi, F. L.; Shyu, S. S.; Chen, C. T.; Lai, J. Y. Polymer 2002, 43, 757.
22. Mi, F. L.; Shyu, S. S.; Chen, C. T.; Schoung, J. Y. Biomaterials 1999, 20, 1603.
23. Quellec, P.; Gref, R.; Perrin, L.; Dellacherie, E.; Sommer, F.; Verbavatz, J. M.; Alonso, M. J. J Biomed Mater Res 1998, 42, 45.
24. Lamprecht, A.; Ubrich, N.; Hombreiro Perez, M.; Lehr, C.-M.; Hoffman, M.; Maincent, P. Int J Pharm 1999, 84, 97.
25. Sun, Y.; Wan, A. J. J Appl Polym Sci 2007, 105, 552.
26. Xu, Y. M.; Du, Y. M.; Huang, R. H.; Gao, L. P. Biomaterials 2003, 24, 5015.
27. Loubaki, E.; Ourevitch, M.; Sicsic, S. Eur Polym J 1991, 27, 311.
28. Yu, J. H.; Du, Y. M.; Zheng, H. J Wuhan Univ (Nat Sci Ed) 1999, 45, 440.
29. Khalid, M. N.; Agnely, F.; Yagoubi, N.; Grossiord, J. L.; Couarraze, G. Eur J Pharm Sci 2002, 15, 425.
30. Borges, O.; Borchard, G.; Verhoef, J. C.; de Sousa, A.; Junginger, H. E. Int J Pharm 2005, 299, 155.
31. Sarmento, B.; Ferreira, D.; Veiga, F.; Ribeiro, A. Carbohydr Polym 2006, 66, 1.
32. Kittur, F. S.; Harish Prashanth, K. V.; Udaya Sankar, K.; Tharanathan, R. N. Carbohydr Polym 2002, 49, 185.
33. Qi, L. F.; Xu, Z. R.; Jiang, X.; Hu, C. H.; Zou, X. F. Carbohydr Res 2004, 339, 2693.
34. Tang, E. S. K.; Huang, M.; Lim, L. Y. Int J Pharm 2003, 265, 103.
35. Gan, Q.; Wang, T.; Cochrane, C.; McCarron, P. Colloids Surf B 2005, 44, 65.